



University of Twente
The Netherlands

Growth & Characterization of p-type Transparent Oxide Semiconductors

Master of Science Thesis
Applied Physics

Ard Vlooswijk
February 2005

Graduation Committee
prof. dr. ing. Dave H.A. Blank
dr. ing. Guus Rijnders
ir. J. Matthijn Dekkers
dr. ir. H.J.W. Zandvliet



Inorganic Materials Science
Faculty of Science and Technology

Abstract

Thin films of Transparent Oxide Semiconductors (TOS) are grown and characterized. The investigated materials are an amorphous n-type TOS: Tin-doped IndiumOxide (ITO, $\text{Sn:In}_2\text{O}_3$) with a optical band gap of 3,5-3,9 eV and a conductivity of 3 kS/cm. A crystalline p-type: CopperAluminiumOxide (CAO, CuAlO_2) with a band gap of 3,3-3,9 eV and a conductivity of 0,38 S/cm. And an amorphous p-type: ZincRhodiumOxide (ZRO, ZnRh_2O_4) with an optical band gap ~ 2 eV and a sheet resistance of 2,5 k Ω .

Thin films are prepared by Pulsed Laser Deposition (PLD). For this process, target materials are prepared using solid-state reactions. The electrical, optical and structural properties of the thin films are determined. The amount of free charge carriers and the scattering of those charge carriers determine the electrical and optical properties. For CAO the crystal structure strongly influences these two factors. In the PLD-process the growth temperature and the oxygen pressure are the most important parameters. For amorphous ITO the presence of oxygen vacancies is most important. For the PLD-process this means the oxygen pressure during deposition is a very important parameter. For amorphous ZRO structure is not important.

Table of Contents

Abstract.....	2
Table of Contents.....	3
List of symbols & abbreviations	4
Introduction	5
1 Theory.....	6
1.1 Transparent Oxide Semiconductors.....	6
1.1.1 General TOS properties	6
1.1.2 Transparency & charge carriers.....	7
1.1.3 Mobility & scattering.....	8
1.1.4 Structural properties.....	10
2 Experimental.....	11
2.1 Synthesis.....	11
2.1.1 TOS thin films	11
2.1.2 Energy of Formation	12
2.1.3 TOS PLD targets.....	13
2.2 Analysis & characterization.....	15
2.2.1 Electrical	15
2.2.2 Optical.....	16
2.2.3 Structural.....	17
2.2.4 Morphological.....	17
3 IndiumTinOxide (ITO).....	18
3.1 Preparation	18
3.1.1 Substrate.....	18
3.1.2 Pulsed Laser Deposition.....	18
3.2 Results	19
3.3 Discussion.....	22
4 CopperAluminiumOxide (CAO).....	23
4.1 Preparation	23
4.1.1 Target.....	23
4.1.2 Substrate.....	24
4.1.3 Pulsed Laser Deposition.....	25
4.1.4 Annealing	26
4.2 Results	26
4.3 Discussion.....	30
5 ZincRhodiumOxide (ZRO).....	31
5.1 Preparation	31
5.1.1 Target.....	31
5.1.2 Pulsed Laser Deposition.....	31
5.2 Results	32
5.3 Discussion.....	34
6 Conclusions	35
7 Literature list	36
8 Appendix	38
8.1 Optical band gap determination.....	38
8.2 Crystal structures	39

List of symbols & abbreviations

Listed here are the often-used symbols and abbreviations in this thesis report. Trivial and/or standardized (SI) symbols are not mentioned in this list, unless their meaning can be confusing.

symbol	meaning	unit	remark
CAO	CopperAluminate		CuAlO ₂
d	thickness	m	
D _n	wavenumber region	m ⁻¹	v ₁ -v ₂
FoM	Figure of Merit	Ω ⁻¹	
ITO	Tin-doped IndiumOxide		Sn:In ₂ O ₃
n	majority charge carrier density	m ⁻³	n-type
p	majority charge carrier density	m ⁻³	p-type
PLD	Pulsed Laser Deposition		
R	total visible Reflectance	-	0-1
R _s	sheet resistance	Ω/□	
RT	room temperature		298 K
T	temperature	°C or K	
T	total visible Transmission	-	0-1
TOS	Transparent Oxide Semiconductor		
μ	charge carrier mobility	m ² /Vs	
V	Voltage	Volt	
V _H	Hall voltage	Volt	
XRR	X-Ray Reflectivity		
ZRO	ZincRhodiumOxide		ZnRh ₂ O ₄

Introduction

This report is a summary of my graduation work performed in the Inorganic Materials Science Group at the University of Twente. My motivation to perform this research is my interest in materials science, combined with my interest in solar energy. This graduation assignment has a rather exploratory character. First an amorphous n-type TOS was grown and characterized: Tin-doped IndiumOxide (ITO, $\text{Sn:In}_2\text{O}_3$). Then a crystalline p-type TOS was grown at elevated temperatures: CopperAluminiumOxide (CAO, CuAlO_2). And finally an amorphous p-type TOS was investigated: ZincRhodiumOxide (ZRO, ZnRh_2O_4).

The reason for this is to understand the relation between structure and properties of TOS materials. With this knowledge p-type TOS thin film growth at low temperatures can be achieved.

From a scientific point of view, it is fascinating to study and grow TOSs, since history has shown that the constant interplay between theory and practice give a good insight in the search for new TOSs and other functional materials. From a commercial point of view it is very interesting to be able to produce p-type TOSs. While industry is already able to produce n-type amorphous TOSs, this is not (yet) the case for p-type TOSs. Thus n-type transparent semiconductors can be produced rather cheap: at low temperatures (room temperature) and on cheap substrates (plastics, glass). The very few p-type TOSs discovered up to now are mostly crystalline TOSs. Amorphous p-type TOSs would open up doors to completely transparent electronics produced in a cheap process. Of course consumer electronics is one of the most important applications of TOSs, only think of the numerous applications of displays. But TOSs are also applied in solar cells, as functional window coatings, etc.

The above-mentioned materials choice is inspired by the current developments in the area of TOS-research. In short, one can state that different metal oxide structures are grown in order to get an electronic structure in which charge transport can take place easily. A lot of different (multi)metal oxides are investigated [20]. Besides these materials being intrinsic semiconductors, doping can increase their electrical conductivity. Doping can be a substitution at a metal-atom site (group III and IV and rare earth) and/or at an O-atom site (group VII). Up till now, their properties are no better than the commercially most applied TOS: ITO. Whereas ITO is n-type, there is no suitable p-type TOS yet being used in applications. Therefore, new materials are being investigated and existing materials are doped in order to obtain a p-type TOS.

An interesting class of materials are the delafossite structure CuMO_2 materials, of which CuAlO_2 is one [26]. This delafossite structure shows an interesting characteristic: it has Cu-layers that are important for the conductivity and it is a p-type semiconductor. CuAlO_2 is chosen since it's often reported in literature (both in bulk as thin film) thus it can be investigated efficiently. A positive aspect for practical applications of CuAlO_2 would be the good availability of aluminium. Even more interesting is ZnRh_2O_4 , as it is shown to be an amorphous p-type TOS. The big interest is caused by the fact that this material is the only amorphous p-type TOS reported so far. A disadvantage for applications is the fact that pure Rhodium is a very rare material and thus extremely expensive.

In this thesis you'll find a theoretical part that describes the different properties of TOSs (1). The next chapter is on the experimental aspects of thin films and their characterization (2). This is followed by chapters on the different materials of which thin films have been produced: successively ITO (3), CAO (4) and ZRO (5). In chapter 6 the conclusions from this research are presented. The report is finished with a literature list (7) and appendix (8) as additional information sources.

1 Theory

This theoretical chapter starts with a general introduction on the theory of TOSs (1.1.1), followed by a section on the combination of transparency and the presence of charge carriers. In section 1.1.3 the mobility of these charge carriers is described. And this chapter concludes with the relation between (crystal) structure & materials properties.

1.1 Transparent Oxide Semiconductors

Because of the different electronic structures of semiconducting materials, they have different band gaps. The band gap of a material is characteristic and quite important for the kind of application it can be used for. The characteristics of a so-called Transparent Oxide Semiconductor (TOS) are an interplay between two opposite effects. These oxides have a specific optical band gap so they can transmit light (large enough energy gap) and conduct electrons (small enough energy gap). To optimise this it's very important to investigate different materials and understand the effects by which their band gap is determined.

1.1.1 General TOS properties

As it's name states, a Transparent Oxide Semiconductor (TOS) has to be transparent. It can be transparent for different applications thus for different parts of the spectrum. For display applications it's optimised for the human eye whereas for applications like solar cells, for the solar spectrum (Figure 1). The human eye is most sensitive to what we call "visible light" which is radiation with a wavelength between 380 nm (3,26 eV) and 750 nm (1,65 eV). The sun emits light with the spectrum shown below, which clearly shows a decreased intensity at 930nm and higher. The semiconductivity of a TOS is defined by the band theory of solids. This theory distinguishes between materials with energy levels far apart (insulators), overlapping levels or bands (metals) and levels apart but close enough for thermal or other excitations to bridge the gap (semiconductors). This energy gap of semiconductors is between 0 and 4 eV.

In Figure 1 this minimum wavelength for materials to be semiconducting (red line) and the maximum wavelength to be transparent (yellow line) are shown. This will be further explained in the next two sections.

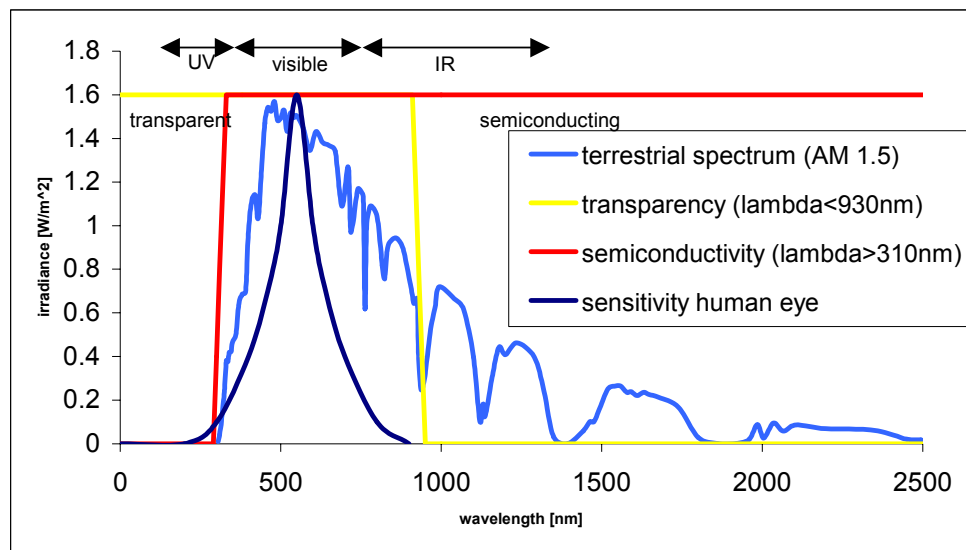


Figure 1: The solar spectrum on earth, sensitivity of the human eye and the properties of transparent and semiconducting materials

For practical applications the transparency and semiconductivity can be numerically expressed in one quality expression: the Figure of Merit (FoM). This number gives an indication to compare the quality of TOSs:

$$(a) \quad \frac{\sigma}{\alpha} = -\frac{1}{R_s \ln(T+R)}$$

in which the electrical properties (R_s) are united with the optical properties (T, R). A larger value of the FoM indicates a better performance of the TOS. The best FoMs achieved in this research are $1,60 \Omega^{-1}$ for ITO, in the order of $10^{-4} \Omega^{-1}$ for CAO and $10^{-3} \Omega^{-1}$ for ZRO.

Besides this subjective number to express the materials qualities, some other, even more subjective, practical aspects are of big importance too. A TOS material should for example be chemically stable and corrosion resistive. Also non-toxicity is a big advantage, which often goes together with the material or its constituents being non-rare and/or inexpensive. In every materials choice these aspects should be kept in mind and are a criteria of arbitrary importance.

1.1.2 Transparency & charge carriers

Transparency is best described by the size of the direct band gap (direct, so no change of quantum number k). This is the minimum energy an incoming photon needs to promote an electron from the valence to the conduction band. This should be high in the “visible” range. Because as long as the photon can’t interact with the material, the material transmits (or reflects) the photon, i.e. the material is transparent. The optical band gap determines the lower band gap limit of a TOS:

$$(b) \quad \lambda_{bg} = \frac{hc}{E_{gap}}$$

Which states that a low band gap wavelength implies a large band gap thus little (light)energy is absorbed. Whereas a large band gap wavelength means a small band gap and a lot of (light)energy is absorbed. As shown in Figure 1 the transmittance should be high from 350 up to 800 nm (this is an indication since the transparent/absorbing transition can’t be abrupt). The upper band gap wavelength limit for transparency, limits the charge carrier density.

For a crystalline material the theoretical maximum charge carrier density, can be calculated from the Drude Theory of Metals (p.18 of [2]). The plasma frequency (as defined in this theory) gives the wavelength for which a material becomes transparent:

$$(c) \quad \omega_p^2 = \frac{4\pi ne^2}{m}$$

which can be expressed to make the relation between carrier density and transparency wavelength more clear like:

$$(d) \quad n = \frac{m\pi c^2}{\lambda_p^2 e^2}$$

This formula seems to give a rather good indication of the radiation wavelength for which alkali metals are transparent. For other materials like TOSs this match is not very good, but it can give at least an estimate (p.19 of [2]). Numerically, the mentioned formulas can be used to calculate the wavelength below which the material will be transparent and the accompanying free charge carrier density (p.18 and 757 of [2]).

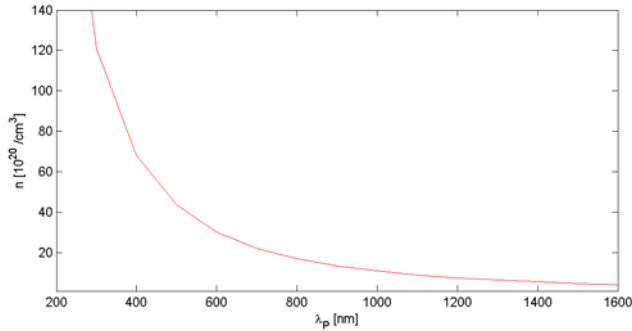


Figure 2: The majority charge carrier density as a function of the plasma wavelength of metals

Figure 2 makes clear that the theoretically maximum obtainable carrier density is of the order $10^{21} / \text{cm}^3$. In practice this limit is only reached for fully optimised thin film growth.

The band gap is also limited by the fact that the TOS has to be semiconducting: a band gap between 0 and 4 eV. So the maximum band gap limits the wavelength with a minimum of approximately 310 nm. Though the transparency would be very poor, the theoretical maximum charge carrier density would be increased to $10^{22} / \text{cm}^3$. The charge carrier concentration increases by increasing the temperature and the effective mass of the charge carriers (p.757 of [2]). The methods to measure the charge carrier concentration are described in section 2.2. The electrical properties of a semiconductor are besides the charge carrier density, also strongly dependent on the charge carriers' mobility (μ) expressed in equation e.

$$(e) \quad \sigma = ne\mu$$

The mobility will be discussed in the next paragraph.

1.1.3 Mobility & scattering

Scattering influences the mobility of charge carriers: the moving charge carriers are scattered by neutral impurities, ionised impurities, grain boundaries and structural disorder.

For n- and p-type TOSs different scattering models are used: for n-type excited electrons take care of electrical conduction in the conduction band whereas for p-type often a hopping mechanism (small polaron as mentioned in [17]) is proposed. This means the scattering of holes and electrons differ, thus their mobilities differ.

For a doped TOS, the ionised impurity scattering is important for the charge transport. The doping can decrease the resistivity since the Coulomb interaction between the ionised (donor) impurities and free electrons are a scattering source intrinsic to the doped material [8].

For all systems, imperfections in the crystal structure like defects and grain boundaries influences the charge carrier transport by scattering. Thus for all TOSs, unintended chemical impurities and crystal imperfections contribute to a lower charge carrier mobility and density.

The main focus for metal oxides is on the O^{2-} ions that have an electronic structure that quite easily donates electrons. So the electronic structure has to be adjusted to overcome this. This is strongest influenced by 3 factors: the kind of metal, the structure of the material and the place of the oxygen and metal atoms with respect to each other in the structure. This will be treated in further detail in the next section.

In practice, the charge carrier mobility is expressed in the Hall mobility μ by

$$(f) \quad \mu = \frac{e\tau}{m_c^*}$$

Which can be increased by either increasing the relaxation time τ or reducing the effective mass m_e^* . Increasing τ is done by making (crystalline) films in which not much scattering can take place, whereas reducing m_e^* is done by finding new materials with charge carriers with lower effective masses. The methods to measure the charge carrier mobility are described in section 2.2.

1.1.4 Structural properties

In this section the relation between structure and properties of the investigated TOSs is shortly explained. The crystal structure of a material is determined by thermodynamic processes. Some of these structures are a very suitable matrix in which conduction can take place. But also materials consisting of very small crystals (nanocrystalline materials) can show quite good electrical properties. Amorphous materials don't show any structure at all, but often the nanocrystalline materials are called amorphous, since for both their crystal structure is not clearly present. In order to grow p-type TOS at room temperature, structure should be of less importance. The reason for this is that metal oxides grown at room temperature show hardly any crystal structure. But in order to understand the properties of nano-crystalline materials, their crystalline phase is also grown and studied.

Besides the fact that it's very hard to theoretically predict which crystal structure will appear when certain atoms are brought together, it's also hard to theoretically calculate the properties of certain structures. The latter of the two is done with the Hartree Fock theory, which is quite well able to calculate properties of simple structures. But for compounds, the theoretical predictions are less accurate. Another problem arising in the case of RT deposition of TOS thin films is the amount of remanence of the crystalline properties in the nanocrystalline state. The crystalline structures of the investigated materials are shown below.

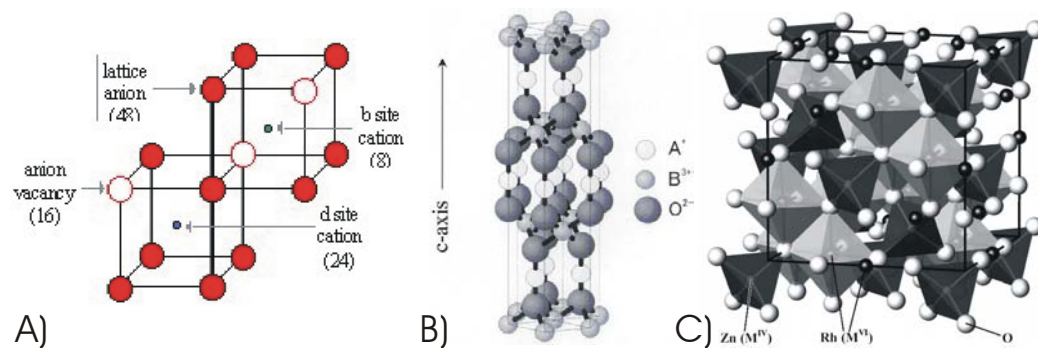


Figure 3: Crystal structures of a) In₂O₃ (oxygen is red, structural vacancies are white and Indium or Tin are grey, from reference [11]); b) CAO (A is copper and B is aluminium, from [19]); c) ZRO (from reference [25])

In₂O₃ grows in a cubic bixbyite structure with a kind of “structural vacancy”, as shown in Figure 3a. The structure of ITO is similar with the Sn-doping substituting In, thus Sn is mainly found on In-sites.

CAO has the delafossite structure shown in Figure 3b. It has a 2D-structure and the conduction characteristically takes place in the copper planes [26]. This structure has two clear disadvantages. First, a 2D-structure retains less of its conduction characteristics than 3D-structures, both in a polycrystalline or nanocrystalline phase. Second, research on similar materials has shown that vacancies on copper positions are often observed. Since the conduction takes place in the copper planes, this decreases the conductivity strongly.

ZRO grows in the spinell phase when it is grown crystalline (Figure 3c). This structure shows one similarity with the CAO delafossite structure: the octahedral orientation of oxygen around the metal ions. The difference is that it's a so-called three-dimensional lattice, which means it has a structure in three dimensions, instead of two, like the copper planes in CAO. This is advantageous for the reason mentioned in the previous paragraph. This is at least the explanation found in literature [22]. From an intuitive point of view, this is a quite likely explanation, but no clear empirical evidence for it has been found.

2 Experimental

In section 2.1 of this chapter the experimental aspects of the synthesis of TOS materials and the growth of thin films is described. In the second part, section 2.2, the characterization of the thin films is described.

2.1 Synthesis

The present atoms, ions and molecules and the state variables related to the available energy determine the formation of a certain material. For equilibrium situations, the present energy is expressed by the Gibbs Free Energy. For specific materials, its state (thus its energy) is represented in a phase diagram, better known as an Ellingham diagram. For metal oxides, this shows the formation temperature of a certain phase as a function of oxygen (partial) pressure. For non-equilibrium situations, the kinetic energy of the particles determines which phase is formed. The kinetic energy is also mainly determined by temperature and pressure.

2.1.1 TOS thin films

Thin films of ITO, CAO and ZRO have been produced by Pulsed Laser Deposition (PLD). The main principles of PLD are shown in figure RR, an extensive description can be found in reference [7]. Though other methods like sputtering, spin-coating and CVD, are also suitable to produce thin films of these materials, all depositions have been performed by PLD. First of all, a physical deposition method is preferable, since most chemical deposition methods operate at a minimum temperature of 200-300°C, whereas sputtering and PLD can be performed at room temperature. The three main reasons for PLD are first of all the good control of growth parameters over a wide range of values, especially the control of the oxygen partial pressure, energy density on the target and substrate temperature. Second, PLD assures a good stoichiometric transfer of the target material. And last, the high kinetic energy of the ablated particles can be advantageous for RT growth since the high mobility of the particles can show similarities with high temperature growth.

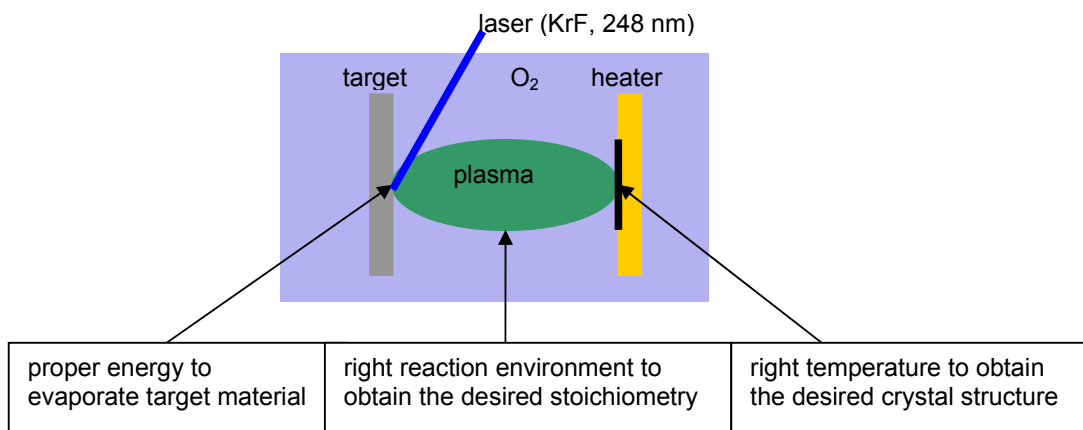


Figure 4: Schematic representation of the PLD process

To control the thin film growth from a plasma phase is not very simple though. Ellingham diagrams give information about the necessary energy to form a certain (crystal) phase of the constituting atoms. But this information is obtained from single crystal growth, whereas thin film growth is performed now. The circumstances during thin film growth are comparable to single crystal growth: it is held at a certain temperature in a certain oxygen pressure. But there are some big differences that can influence the crystal growth strongly. First of all the material comes from a highly supersaturated gas phase, a plasma, and “ripens” onto a substrate. Second, the (initial)

phase formation on this substrate depends strongly on the character of the substrate: amorphous or crystalline resulting in epitaxial growth. And last, the deposition process is not an equilibrium state, so the thermodynamic laws are not valid, but some quasistatic approximations or thermodynamic laws describe the process.

The situation described in the Ellingham diagram can be approached closely by using a substrate with a perfect lattice match to the crystalline thin film and leaving this for a long time at the desired temperature and p_{O_2} (annealing). Though this is unwanted since low-temperature growth by PLD without any anneal is preferred.

2.1.2 Energy of Formation

In this section the relation between energy and crystal phases is described which is the starting point for the next section. In the next section the synthesis of PLD targets is described.

The ideal circumstances for crystals to form, can be calculated using formation energies of the different crystal structures. The Gibbs free energy (G) is a state function and it predicts whether a process will occur spontaneously (or not) at constant (oxygen) pressure and temperature. The change in Gibbs free energy that accompanies the formation of one mole of a compound (from its elements) indicates which phase will form:

$$(g) \quad dG = dU - TdS - SdT + PdV + VdP$$

For a given reaction $M + O_2 \rightleftharpoons MO_2$ this change indicates:

$dG < 0$, the reaction is spontaneous as written (i.e. goes to the right) ;

$dG > 0$, the reaction will proceed to the left;

$dG = 0$, the reaction is at equilibrium ;

In practice, fortunately, a lot of parameters disappear from equation g since they are constant. This is not the case for the system during growth of thin layers of material: the plasma exchanges both matter and energy with the substrate. But after deposition a constant temperature, pressure, volume and amount of material is present. Thus a system kept in this state for a while will reach equilibrium and a certain phase will appear. For this reason often annealing is performed after the growth. In this equilibrium state the system will always strive to minimize the Gibbs free energy G , thus $dG=0$. And dG can be described by

$$(h) \quad dG = dH - TdS$$

So the actual deposition is mainly important to obtain the right stoichiometry of the metals and the (in-situ) annealing is to get the right reaction with oxygen (O_2) to form a crystalline metal oxide. Of course this reaction with oxygen already occurs during deposition, but it is best controlled during post-anneal since there's an equilibrium situation. And in case there's a system with several possible reactions and resulting products, not only the sign is important, but simply the difference in change in Gibbs free energy.

The Gibbs free energy associated with different crystal phases of materials is usually represented in Ellingham diagrams. They show how the temperature and oxygen partial pressure are related to different crystal structures. Generally, for a given reaction ($M + O_2 \rightleftharpoons MO_2$) and assuming that the activities of M and MO_2 are taken as unity, the following equations can be used to express the oxygen partial pressure at which the metal and oxide coexist, i.e. the dissociation pressure of the oxide:

$$(i) \quad p_{O_2}^{M/MO_2} = e^{\frac{\Delta G_0}{RT}}$$

or its logarithmic form

$$(i \text{ II}) \quad \log(p_{O_2}^{M/MO_2}) = \frac{\Delta G_0}{2,303 \cdot RT}$$

This is plotted for CAO in Figure 5. For In_2O_3 and ZRO no Ellingham diagrams or Gibbs Free Energy data were found in literature.

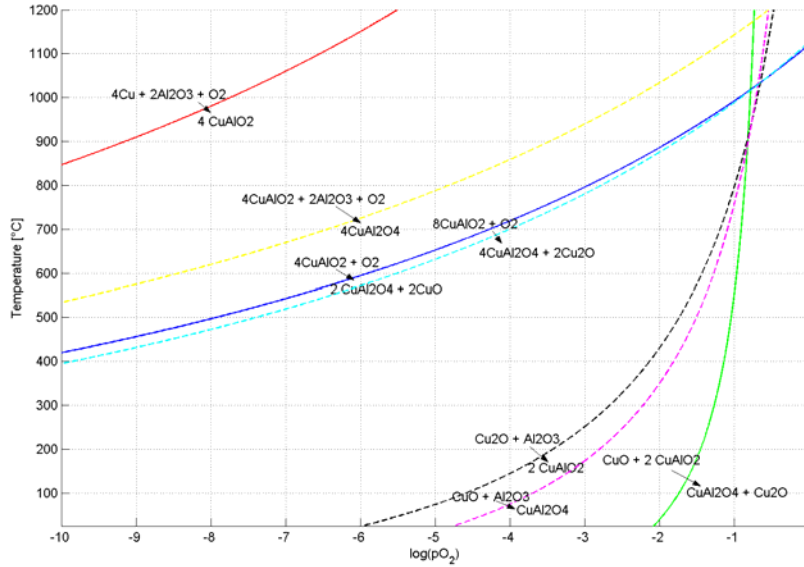


Figure 5: Ellingham diagram of the Cu-Al-O system, showing a large amount of different phases. These different phases even show a lot of coexistence indicating a lot of multiple-phase growth (from reference [9] and [15])

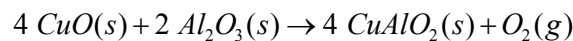
2.1.3 TOS PLD targets

Targets for PLD are stoichiometric pieces of the material to be deposited as a thin film. Since PLD takes place in a vacuum chamber with controlled oxygen content, the oxygen is not necessarily present in a stoichiometric proportion in the target, unlike the other elements.

A way to produce these targets is by a solid-state reaction. This process is described here for CAO and ZRO. In fact, what happens in a solid-state reaction is that the material is brought to the desired equilibrium situation described in the Ellingham diagram. In this way the desired crystal structure is formed.

To obtain a CAO-target with the right stoichiometric proportions, Cu and Al should be present in a 1:1 proportion. Perfect oxygen content is not inevitable, since the oxygen pressure adjusts the oxygen content in the thin film during the deposition process.

In literature, several routes are described to prepare bulk CuAlO_2 (hydrothermal, solid state etc.). The method described by Stauber et al. [28] is used because of its simplicity and good results. In fact this is a solid-state reaction of a 2:1 molar mixture of CuO and Al_2O_3 powders:



The reported sintering temperature differs in literature from 1000 to 1200°C. For target I the powders were pressed to a pellet which was sintered. For target II the powders were first sintered and then a pellet was pressed and sintered. These processes are described in more detail in the next table.

Experimental details CAO target preparation

Powders	
CuO	Aldrich 99+% purity Copper(II)Oxide, particle size < 5 μm
Al ₂ O ₃	Sumitomo AKP50 particle size <0,6 μm
Preparation target I	
Mix powders	- 13,2589g CuO and 8,4975g Al ₂ O ₃ were mixed with 22ml ethanol and 65g ZrO ₂ grinding balls. This was mixed for 24 hours in a ball miller and then dried and sieved.
Press pill	- 3 minutes at 6,5 Mpa uniaxially, then 2 minutes isostatically at 400 Mpa
Sintering	- 10hrs at 1000°C; slope 2°C/min
Regrind, repress	- as above
Sintering	- 10hrs @ 1055°C; slope 2°C/min
Regrind, repress	- as above
Sintering	- 15hrs @ 1100°C; slope 2°C/min
Result	- CAO target with a relative density of 67%
Preparation target II	
Mix powders	- 13,259g CuO and 8,498g Al ₂ O ₃ were mixed with 22ml ethanol and 65g ZrO ₂ grinding balls. This was mixed for 24 hours in a ball miller and then dried and sieved.
Sinter powders	- 15 hours at 1100°C; slope +10 -3°C/min
Press pill	- 3 minutes at 6,5 Mpa uniaxially; then 2 minutes isostatically at 400 Mpa
Sintering	- 15 hours at 1100°C; slope +10 -3°C/min
Regrind, repress	- as above
Sintering	- 15 hours at 1100°C; slope +10 -3°C/min
Result	- CAO target with a relative density of 67%

For a good stoichiometry of the ZRO-target, Zn and Rh should be present in a 1:2 proportion. As mentioned before, perfect oxygen content is not inevitable. The solid-state route to prepare a target, as described in reference [21] and [27], is used here:

Experimental details ZRO target preparation

Powders	
ZnO	Alfa Aesar 99,99% purity Zinc Oxide
Rh ₂ O ₃	Alfa Aesar 99,9% purity Rhodium(II) Oxide anhydrous
Preparation target I	
Mix powders	- 2,0451g Rh ₂ O ₃ and 0,6561g ZnO were mixed with 2,6ml ethanol and 8 grams ZrO ₂ grinding balls. This was mixed for 24 hours in a ball miller and then dried and sieved.
Press pill	- 3 minutes at 11,9 Mpa unistatically; then 2 minutes in oil at 400 MPa
Sintering	- 5hrs at 800-1000°C with 1°C/min slope
Regrind, repress	- as above
Sintering	- 4hrs at 900°C with 1°C/min slope
Result	- XRD figH, relative density 51% of ZRO

2.2 Analysis & characterization

The different methods to characterize thin TOS films and the accompanying measurement set-ups are described in this paragraph. Treated are successively electrical, optical, structural and morphological methods of analysis and characterization.

2.2.1 Electrical

Three different kinds of electrical measurements were performed in a general set-up:

Four-point Van der Pauw setup to measure the resistance.

Resistivity measurements can be performed with the simple set-up shown in Figure 6. From the VI-data from the different terminals and a separate thickness measurement, the sheet resistance can be calculated numerically from

$$(j) \quad e^{-\pi R_A/R_s} + e^{-\pi R_B/R_s} = 1$$

and the electrical conductivity from

$$(k) \quad \frac{1}{\sigma} = \rho = R_s d$$

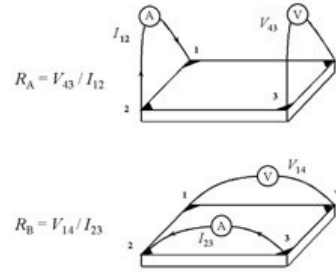


Figure 6: 4-point Van der Pauw set-up (from [24])

Four-point Van der Pauw setup in a varying magnetic field to measure the Hall mobility and determine the type of semiconductor (n or p).

This measurement can be performed with a van der Pauw set-up in a perpendicular magnetic field, shown in figure 7. From the VI-data and the magnetic field, the charge carrier density and type can be determined. The principle of the Hall effect is the Lorentz force whereby a magnetic field B exerts a force on a moving charged particle. The Lorentz force is perpendicular to the direction of propagation of charge carriers and the magnetic field B . Hence an electron moving through a bar of semiconductor will be deflected to one side and generate a voltage V_H .

$$(l) \quad \vec{F}_L = -q \cdot \vec{v} \times \vec{B} \text{ (Lorentz force)}$$

The resulting Hall voltage is:

$$(m) \quad V_H = \frac{I \cdot B}{n \cdot q \cdot d}$$

Holes and electrons propagate in opposite direction with opposite charge and are therefore deflected toward the same side. In this way it is possible to identify the majority charge carrier in a semiconductor. Since the Hall voltage is positive for p-type semiconductors with holes as major carriers and negative for n-type. Now the charge carrier density and conductivity are measured, the mobility μ can also be determined with above formulae from the simple relation

$$(n) \quad \sigma = n_e e \mu_e + n_h e \mu_h$$

Thus the mobility, charge carrier density and type can be calculated from thickness, electrical resistance and Hall voltage measurements. Besides Hall voltage measurements, the type of charge carriers can also be determined by Seebeck measurements [5].

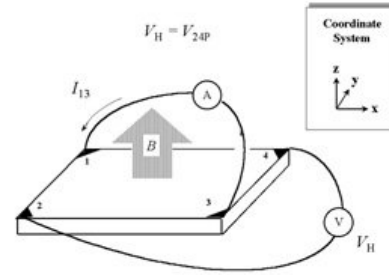


Figure 7: Hall measurement set-up

Two-point setup to measure the sign of the Seebeck coefficient; qualitative method to determine the type of semiconductor (n or p).

By performing a two-point electrical measurement and heating or cooling one of the electrodes (as shown in Figure 8), a thermoelectric current will flow. Since every charge carrier involved in the electric current carries with it some entropy, the sign of the thermoelectric current or voltage contains information about the charge of the charge carrier.

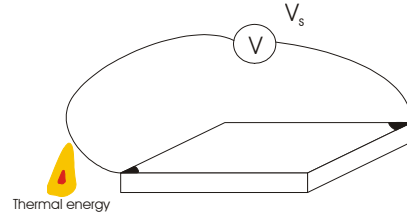


Figure 8: Qualitative Seebeck measurement set-up

2.2.2 Optical

A Cary 50 UV-VIS Varian Inc. spectrophotometer was used to measure the reflectivity and transmittance. This apparatus emits light of a single wavelength incident at a 90° and 45° for transmittance respectively reflectance measurements. The spectrum of only the thin film was obtained by subtracting the spectrum of the substrates by measuring bare substrates ('baselines') too. Transparency and reflectance spectra contain information about the spectral response of a thin film. Two important optical properties of a TOS can be deduced from this: the band gap and the optical transmittance τ . In literature the optical transmittance is defined as the average of the transmittance from 400 to 700 nm. In TOS research there's also a standardized way to determine the optical band gap by measuring the transmittance and reflectance of the film for different wavelengths. Some standard optical calculations (for a deduction the reader is referred to Appendix 8.1) lead to a formula to determine the band gap of a direct band gap semiconductor:

$$(o) \quad \left(\frac{\alpha h\nu}{A} \right)^2 = h\nu - E_g$$

So α^2 is plotted as a function of the energy $h\nu$, which should give, at least in the energy region for which the material is a direct gap semiconductor, a linear relation. And finally the optical band gap is obtained by fitting a straight line to the plot and determining its energy-axis intersection ($\alpha^2=0$, so this gives the band gap energy E_g).

For thin films, spectrophotometer data can also be used to determine the thickness of these films as described in reference [13]. The formula

$$(p) \quad d = \frac{m}{2D_n \sqrt{(n^2 - \sin^2 \theta)}}$$

states the relation between the wavelength and the product of thickness and index of refraction. Thus the index of refraction has to be estimated to determine the thickness. Especially around the band gap, this is not a constant.

2.2.3 Structural

The crystallographic structure of a material is determined by irradiating it with X-rays and measuring the reflected rays. An Enraf-Nonius diffractometer emits Cu K α -radiation. This X-ray radiation is focused and emitted onto the materials surface and its reflection is measured. The resulting spectrum contains information about the structure and content of the first tens of μm of the irradiated surface. An extensive description can be found in reference [18].

The width of the observed peaks in the spectrum contains information about the strain and crystallite size in the material. The Full-Width-Half-Maximum (FWHM) can be used to calculate the particle size with the Scherrer-method:

$$(q) \quad D = \frac{0,9 \cdot \lambda}{FWHM \cdot \cos \theta}$$

The X-ray diffractometer can also be used to determine the thickness and roughness of thin films. This method is called X-ray Reflectivity (XRR) and is based on the reflection of X-rays at very small angles of incidence. From the fall of the reflectivity between two adjacent maxima or minima, the roughness can be determined. The difference in wave vector between two adjacent maxima or minima is a measure for the film thickness. For very small angles, assuming the index of refraction is close to 1 and using Bragg's law and some geometry, one can write

$$(r) \quad q_2 - q_1 = \frac{2\pi}{d}$$

which can be written for practical use like

$$(s) \quad d = \frac{\lambda}{2(\sin \theta_2 - \sin \theta_1)}$$

With θ_1 and θ_2 the angles corresponding to a maximum and the adjacent minimum (or vice versa). An extensive description of this method can be found in reference [1].

2.2.4 Morphological

The morphology of the surface of a thin film can be determined with an Atomic Force Microscope (AFM). An AFM registers the near field force interactions between the surface and a tip mounted on a cantilever beam to determine the surface roughness and possible present structures on the surface of the thin film. It is operated both in contact and in tapping mode. A Digital Instruments Nanoscope IV AFM with SiN tips is used for determination of the thin film surface. It is also used to determine the surface properties of bare substrates used for epitaxial growth. An extensive description of the operating principles of an AFM can be found in reference [3].

To determine the sheet resistance (paragraph 2.2.1) the thickness of the thin film is measured separately. Besides analysing fringes in the optical and X-ray spectra, this is done with an Alpha Step 250 by Tencor Instruments. By moving an AFM-like tip over a step edge, the thickness is measured with a moderate accuracy. This step edge is created by using a deposition mask in the PLD process.

3 IndiumTinOxide (ITO)

ITO is an extensively studied n-type TOS [12],[20], with good properties. The properties reported in literature are a band gap varying from 3,0 to 3,7 eV; transparency of 85-90%, conductivity up to 1000 S/cm, charge carrier density of $1 \cdot 10^{21}$ and a mobility of 10-100 cm^2/Vs .

For PLD, commercial ITO targets with different doping content are available. For this research, targets with 0, 5 and 10wt% Sn-doping in the Indium Oxide are used.

3.1 Preparation

Since ITO also has good properties when it is grown nanocrystalline, depositions can take place at room temperatures. We found earlier [8] that for RT depositions the oxygen pressure during deposition is an important parameter to optimise the materials' properties. In this way the amount of oxygen vacancies can be "tuned" which is an important property of the material.

3.1.1 Substrate

While ITO is deposited at relatively low temperatures, substrates of glass or plastics like PET (Polyethylene Terephthalate) can be used. PET is a plastic of which the temperature should stay below 100°C and it should not be treated with strongly corrosive chemicals. PET is cut in 1x1 cm substrates that are ultrasonically cleaned in acetone and rinsed with ethanol.

Standard quality glass is used to deposit at higher temperatures. Glass can stand temperatures up to 300°C without degassing and reacting too much. At higher temperatures, a lot of degassing occurs and possibly some reaction with the deposited material. Glass is cleaned in the same way as PET.

3.1.2 Pulsed Laser Deposition

Pulsed laser deposition is performed at different temperatures and oxygen pressures to examine the crystallization process and the influence of these important parameters. The experimental details can be found in the table below. Of course, PET was only used for temperatures up to 50°C. All substrates were clamped onto the heater, for high temperatures this might give some fluctuations between the observed (heater) temperature and the real temperature. But these fluctuations are orders of magnitude smaller than the temperature differences between the different films.

Experimental details: PLD-settings

spot size	3 mm ²
energy density	3 J/cm ²
temperature	RT – 500 °C
background pressure	$2 \cdot 10^{-6}$ – $4 \cdot 10^{-5}$ mbar
process pressure and gas	0,005 – 0,030 mbar O ₂
substrate	glass, PET
targets*	In ₂ O ₃ ITO 95/5 wt% (molar content In:Sn:O = 2,00 : 0,12 : 3,00) ITO 90/10 wt% (molar content In:Sn:O = 2,00 : 0,26 : 3,00)

*all targets were obtained from Umicore.

3.2 Results

The ITO thin films were characterized by the methods described in section 2.2.

The resistivity measurements could be performed quite easily with the Van der Pauw set-up. Since the resistivity of these films was not very high, applied currents of a few mA resulted in voltages to be measured in the order of 10 mV. The lowest resistivities were obtained for films deposited at 300°C and oxygen pressures of 0,004-0,008 mbar, namely a sheet resistance of 6,15 Ω/\square for 500nm thick films, meaning a resistivity of $3 \cdot 10^{-4} \Omega \cdot \text{cm}$. most films had resistivities in the order of $1 \cdot 10^{-3} \Omega \cdot \text{cm}$.

The sheet resistance and the optical band gap of ITO 90/10 deposited at an oxygen pressure of 0,020 mbar, is shown in Figure 9. Note that the lines simply connect the points and that for growth temperatures from 100 to 250°C no measurements were performed since the films cracked. The films grown at temperatures up to 100°C are further called nanocrystalline and the ones grown at temperatures above 250°C polycrystalline. The resistivity of these two types of films hardly differs, in a sense that none of the two phases has lower or higher resistances than the other. The sheet resistance shows a “theoretical” minimum around 200°C.

The nano- and polycrystalline samples show different band gaps and optical transmission. The band gap of polycrystalline samples is a few eV higher than that of nanocrystalline samples. The optical transmission of the polycrystalline films is a few percentages higher than the nanocrystalline films (87% versus 81-83%).

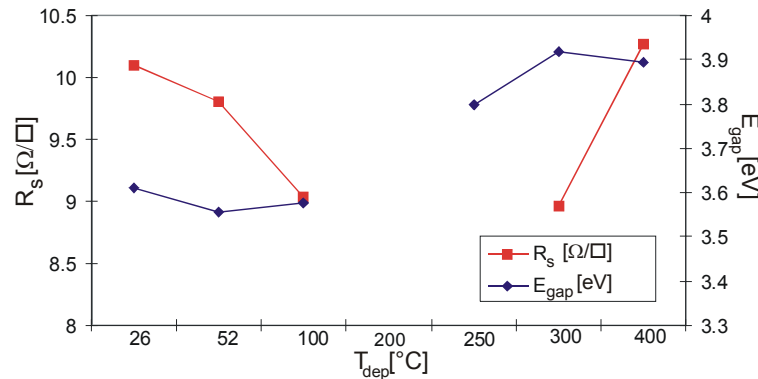


Figure 9: Sheet resistance and band gap of ITO 90/10 films grown in 0,020 mbar oxygen pressure and different temperatures

Resistivity and transmission measurements of thin films of ITO 90/10 grown at 300°C on glass show strong oxygen pressure dependence (Figure 10a). Both the transmission and the resistivity are optimised at an oxygen pressure of approximately 0,007 mbar.

RT-grown films for different doping contents show similar strong oxygen pressure dependence (Figure 10b). For RT-grown films the lowest resistivity is achieved for films without Sn-doping. Besides, the optimum oxygen pressure decreases with decreasing Sn-doping.

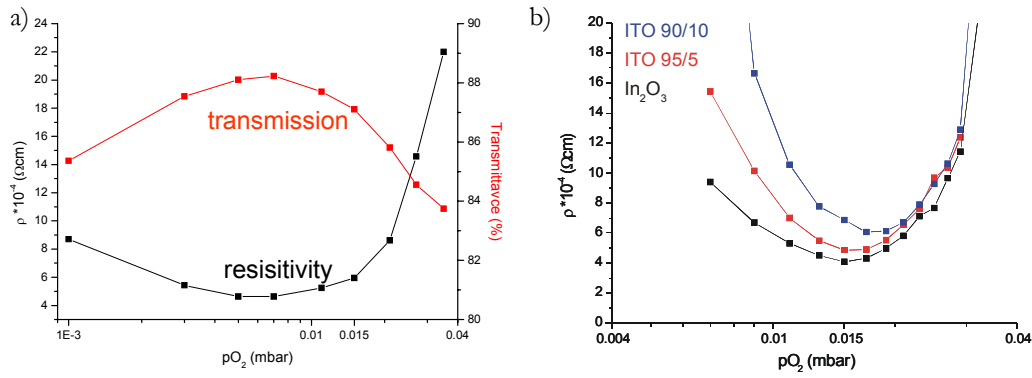


Figure 10: a) Optical transmission and electrical resistivity as a function of the oxygen deposition pressure (of ITO 90/10 grown at 300°C). b) Electrical resistivity of In_2O_3 with different Sn-doping contents and different oxygen deposition pressures.

The difference between doped and undoped In_2O_3 films deposited at RT is shown in Figure 10b. From the field dependence of the current in Hall measurements, the charge carrier density was calculated. Together with the resistivity data the mobility of the charge carrier was obtained. Both are plotted in Figure 11a. The charge carrier density shows a peak for both doped and undoped In_2O_3 , at different oxygen pressures though. The mobility increases with oxygen pressure and shows a possible decrease at relatively high oxygen pressures of $0,035$ mbar. Seebeck measurements were only performed qualitatively, to determine the type of majority charge carrier, which was confirmed to be n-type.

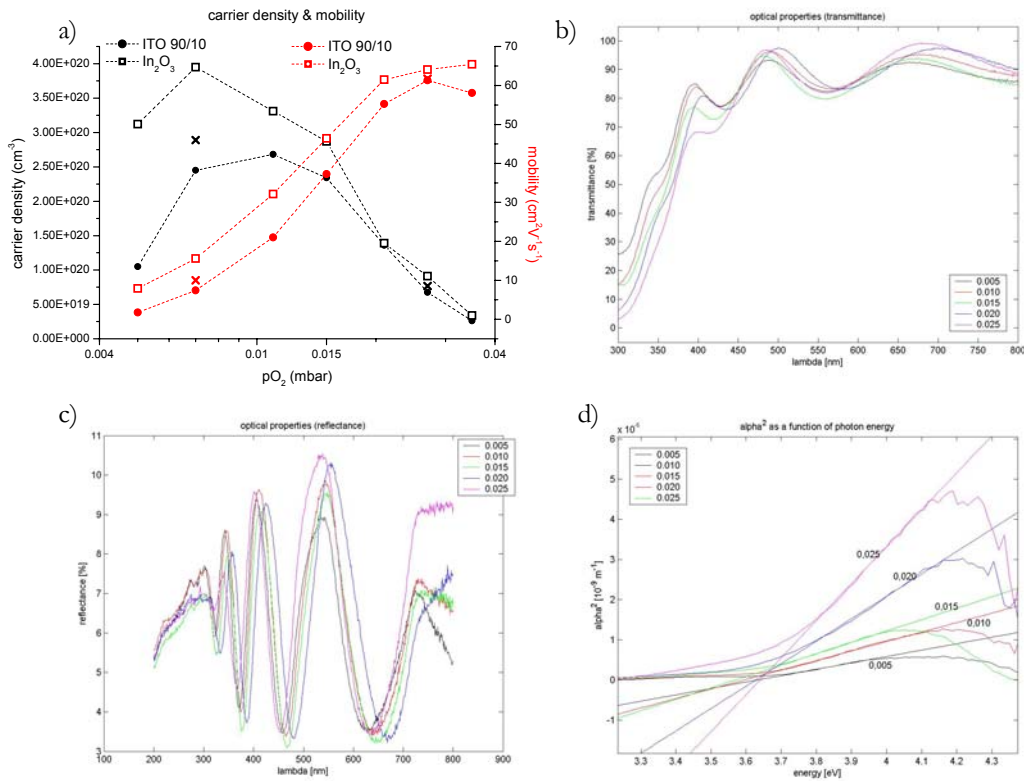


Figure 11: a) Charge carrier density and mobility for different RT-grown films; b-d) optical spectra of ITO 90/10 grown at 300°C and different oxygen pressures.

The optical transmission and reflection spectra of ITO 90/10 grown at 300°C at different oxygen pressures are shown in Figure 11b and c. The fringes are due to the thickness of the thin film. The fringes appearing in the reflectance data indicate a film thickness of 509 ± 82 nm, when a constant index of refraction of 2 is assumed.

Figure 11d shows how the optical band gap is determined. α^2 is plotted against the photon energy and the x-axis cut-off of lines along the steep slope of this graph, indicate the value of the optical band gap. In this case the band gap seems to be decreasing with increasing oxygen pressure.

All the X-ray diffraction spectra of ITO 90/10 deposited at $pO_2=0,020$ mbar and different temperatures, show an increased signal at lower θ values caused by the glass. For 100°C no crystallinity is detected. At 200°C some crystallinity appears. For 300°C this peak is at it's largest to decrease again for 400°C and 500°C. The decrease in crystallinity for temperatures of 400°C and higher is probably caused by reaction of the glass with the deposited material.

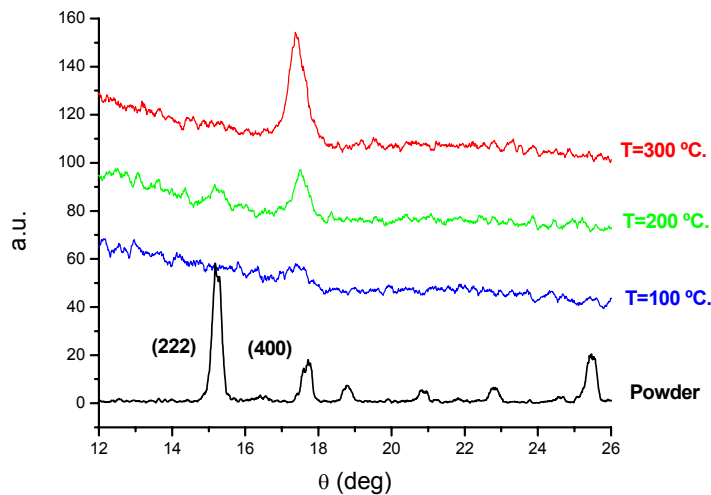


Figure 12: XRD-spectra of ITO 90/10 films grown at different temperatures.

Atomic Force Microscopy shows very flat surfaces for films grown at low temperatures and quite rough ones for films grown above the crystallization temperature. This is what one expects: at low temperatures the atoms do not order in a macrostructure and thus no large clusters will be present. At higher temperatures, the crystalline clusters will cause more surface roughness.

3.3 Discussion

From the results in the previous section it's clear that the growth temperature is an important parameter for the formation of crystal phases. The crystal structure is not necessary for the electrical conduction in ITO. Also for transparency the structure is not needed, but it has more influence on the optical properties than on the electrical properties. Amorphous ITO has a lower band gap than crystalline ITO, thus in the amorphous phase photons are more easily absorbed. This is confirmed by the observation that amorphous ITO has a lower optical transmission. Physically this is represented by (light) waves travelling through a regular structure more easily than an irregular structure.

Besides growth temperature, the oxygen pressure is an important parameter in the determination of the thin film properties. The oxygen pressure in the deposition process is related to the oxygen vacancies in the thin film. Increasing the oxygen pressure decreases the oxygen vacancies and vice versa. As this oxygen pressure strongly influences the electrical and optical properties of ITO, oxygen vacancies play an important role in the conduction.

For a certain amount of oxygen vacancies both the electrical conductivity and the optical transmission show a maximum. By increasing the oxygen vacancies, scattering increases. Thus the mobility of the charge carriers is decreased. But increasing the oxygen vacancies also increases the charge carrier density. In this case the conduction is limited by the charge carrier mobility and not by the charge carrier density. Thus the resistance increases.

By decreasing the oxygen vacancies, the opposite occurs: scattering decreases and the mobility of charge carriers increases. Now the conduction is limited by the charge carrier density and not by their mobility. Thus again the resistance increases.

Also the dopant (Sn at In-sites) can be an important parameter for the electrical properties. For polycrystalline films doping increases the charge carrier density. The electrical properties of amorphous (Sn:)In₂O₃ are not improved by doping.

Doping decreases the mobility. For amorphous films SEM-images show that Sn acts as a nucleation centre during PLD-growth resulting in smaller grain sizes. Thus the Sn itself doesn't act as a scatterer, but it increases the amount of grain sizes resulting in more scattering.

Also the charge carrier density is decreased by doping, but this effect shows an oxygen pressure dependence. For RT-grown films at high oxygen pressures, doping induces hardly any decrease in charge carrier density. At low oxygen pressures, films with different amounts of doping show different charge carrier densities. This is not understood yet. Increase of doping, decreases the charge carrier density. Thus the Sn could act as a neutral impurity, not contributing to the charge carrier density. Also other explanations are possible, like formation of other crystal phases.

The cracks occurring in thin films grown in the range of the crystallization temperature of In₂O₃, can be explained by a simple model: at low temperatures the amorphous film simply forms an independent layer on the substrate. Increasing the temperature up to the crystallization temperature, increases the available energy for crystalline growth. There's sufficient energy for the film to grow crystalline but as soon as temperature gradients occur, strain occurs and causes the film to crack. Increasing the growth temperature more, enhances the crystalline growth. The film obtains enough energy to release strain. This model is supported by the fact that it was observed that the films cracked upon cooling down. But it wasn't verified by measurements.

4 CopperAluminiumOxide (CAO)

CAO is a recently discovered p-type TOS [17]. The material only shows TOS-properties in the delafossite structure. The best properties reported in literature[14] are a band gap of 3,5 eV, a conductivity of 2 S/cm, a charge carrier concentration of $1,3 \cdot 10^{17} \text{ cm}^{-3}$ and a mobility of 10 cm^2/Vs .

4.1 Preparation

In this paragraph the fabrication process of thin CAO films is described. This process starts with the target preparation described in section 2.1.3. Here the analysis of these PLD-targets is discussed. Material of these targets is deposited onto well-treated substrate to form a thin film. To obtain the right crystalline phase in this thin film, annealing has been performed. Other methods to decrease these growth temperatures have been applied. Like growth at extremely low oxygen pressures by mixing gasses and epitaxial growth on a lattice-matched substrate.

4.1.1 Target

The PLD-targets prepared by the method described in section 2.1.3, were analysed before use. X-ray diffraction on this target showed that it consists mainly of CuAlO_2 (Figure 13). But some CuO together with $\text{Al}_2\text{O}_3/\text{CuAl}_2\text{O}_4/\text{Cu}_2\text{Al}_4\text{O}_7$ is present too.

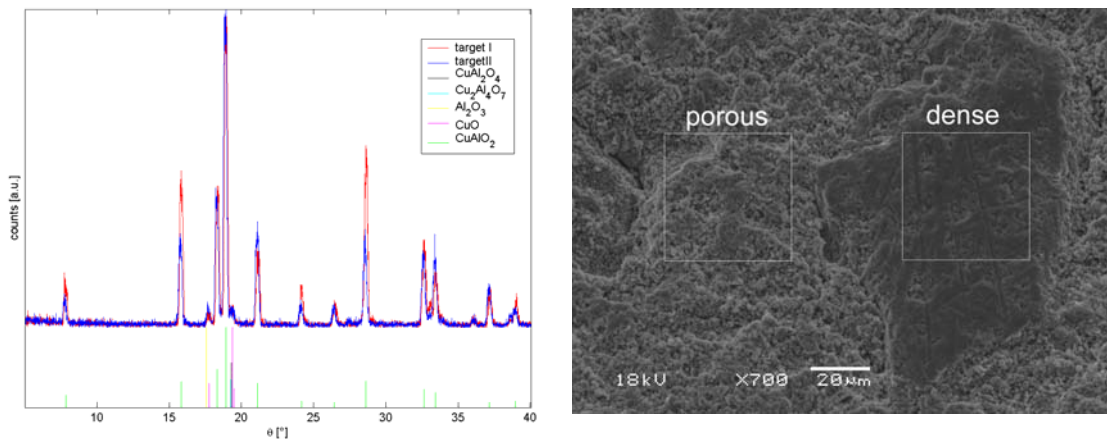


Figure 13: left: XRD-spectra of target I & II and diffraction peaks of possibly present phases; right: SEM-photograph of the target material showing density differences.

XRD-analysis is performed to be sure the right stoichiometric mixture is present in the target. But also the colour and density of the target give some important information. The possible phases are:

phase	colour	ρ [10^3 kg/m^3]	shortage
CuO	black or brown-black	6,31	Al, O
Cu ₂ O	yellow, red or brown	6,00	Al, O
Al ₂ O ₃	White	4,00	Cu, O
CuAlO ₂	light grey	5,06	
CuAl ₂ O ₄	chocolate/wood brown	4,60	Cu
Cu ₂ Al ₄ O ₇			Cu, O

Obtained targets are grey with some brownish spots. This can imply that besides CAO, some CuO, Cu₂O or CuAl₂O₄ is present too.

SEM shows that the density of the target clearly varies within the target (Figure 13). This indicates the presence of amorphous phases or crystalline phases with different densities. Therefore XRF-analysis has been used to be sure the targets have the right stoichiometric proportions. In this XRF-analysis Cu and Al were measured with O balanced to 100%:

target	element	measurement	molar mass	molar content	molar ratio
CuAlO ₂ I	Al	20,41	26,982	0,756	1,000
	Cu	49,38	63,546	0,777	1,027
	O	30,21	15,999	1,888	2,496
CuAlO ₂ II	Al	20,29	26,982	0,752	1,001
	Cu	47,75	63,546	0,751	1,000
	O	31,96	15,999	1,998	2,656

The molar content for target II is 1:1 within the measurement error. Target I seems to have a small off-stoichiometry with a small Al shortage. For both targets there's clearly excess oxygen. So it's quite likely that both targets contain besides CAO some CuO with CuAl₂O₄. Target II has the best Cu:Al stoichiometry.

4.1.2 Substrate

For growth of crystalline CAO thin films, a substrate with an epitaxial fit is necessary. C-cut sapphire is a good material to serve as a substrate. Sapphire (Al₂O₃) is a transparent, non-conducting material and the c-cut has a rather good lattice match to CuAlO₂. The tensile lattice mismatch is 3.7%, which is small enough to overcome by relaxation in the thin film. The c-cut sapphire is thermally treated before use. In this way, an atomically flat surface is formed, with step edges of half a unit cell (see Figure 14). The measured step height for the three shown steps is 0,598 nm. The step height corresponds to half a unit cell of Al₂O₃ in the c-direction. In literature a step height of 0,22 nm is also reported^[31] but this was not observed in this research.

With only a miscut angle of 0,61±0,01°, a surface without any observable defects, and lattice constants that match those of CAO closely, epitaxial growth of CAO on this surface is facilitated. This is illustrated by the crystal data in Appendix 8.2.

Substrate details

5x5 mm c-cut sapphire from SurfaceNet GmBh
 ultrasonic cleaning in acetone
 thermal treatment for 6 hours at 1200°C in atmospheric conditions
 miscut 0,6 °

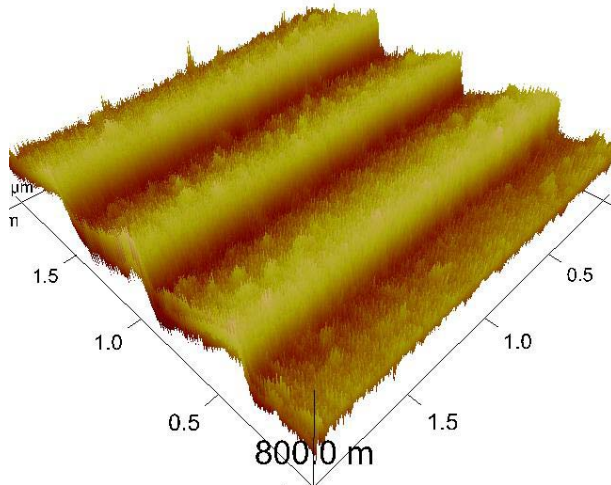


Figure 14: AFM image of a treated c-cut sapphire substrate (note: the z-axis is 0,800 nm).

4.1.3 Pulsed Laser Deposition

For good stoichiometric deposition, first the effect of the energy density on the target is investigated (see Figure 15). It seems that for CAO-depositions with energy fluence of 4 J/cm^2 , good homogeneous ablation takes place without inhomogeneities like pillars forming on the target during ablation. The ablation is still not perfectly homogeneous but it is clearly more homogeneous than at lower fluencies and at higher fluencies not much improvement is observed.

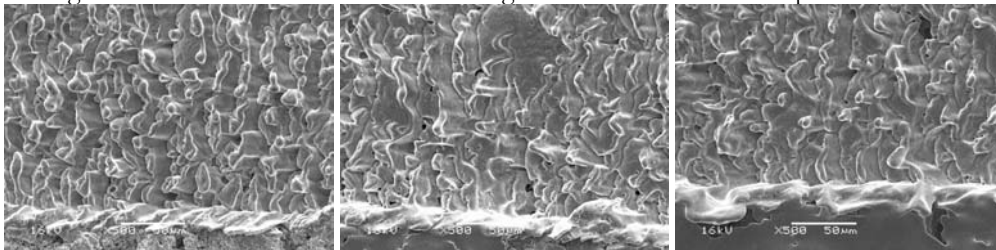


Figure 15: SEM-images of ablated surfaces of a CAO-target. The energy density on the target varies from 2 J/cm^2 on the left via 4 J/cm^2 in the middle to 5 J/cm^2 on the right.

Pulsed laser deposition is performed at different temperatures and oxygen pressures to examine the validity of the Ellingham diagram in Figure 16. The experimental details are mentioned in the table below. Because of the high deposition temperatures, the substrates were glued to the heater with silver glue. This ensures good heat conduction to the substrate so it will have approximately the same temperature as the heater.

Experimental details: optimised PLD-settings

spot size	$2,5 \text{ mm}^2$
energy density	4 J/cm^2
temperature	$750 \text{ }^\circ\text{C}$
background pressure	$1 \cdot 10^{-6} - 4 \cdot 10^{-5} \text{ mbar}$
process pressure and gas	$0,004 \text{ mbar O}_2$
substrate	c-cut sapphire (Al_2O_3)
targets	CAO I & II

4.1.4 Annealing

Since in the PLD process, the material is deposited with a rather high kinetic energy, the thin film is not in thermodynamic equilibrium. The film can reach thermodynamic equilibrium by annealing it at high temperatures. The different equilibrium states for bulk CuAlO_2 are shown in Figure 5. Appropriate deposition conditions can enhance the equilibrium state, though post-annealing seems to be a very effective way to improve the film quality. Based on literature [30], in-situ anneals were performed for 3 hours at deposition temperatures and oxygen pressures.

4.2 Results

On only few CAO samples resistivity measurements could be performed. In the present set-up, no Hall measurements could be performed. Seebeck measurements formed an alternative to determine the type of majority charge carrier. Transparency measurements were hard to perform because of the silver glue involved in the production process. But XRR-measurements gave information on the thickness. XRD and AFM measurements show quite good harmony.

Resistivity measurements of CAO films can only be performed on films with high conductivity. The resistivity of films containing crystalline phases other than CAO, was too high to measure in the current set-up. Some films with the right CAO phase also have too high resistivities to measure. This is indicated in Figure 16. Based on this Ellingham diagram, it is most likely that for these high resistive CAO-films, too many other (non-crystalline) phases are present that disturb the structure in such a way that the conductivity can't be measured.

The resistivities that could be measured, were in the order of $7 \cdot 10^4$ up to $10^6 \Omega/\square$. Thus the best film with a sheet resistance of $7,43 \cdot 10^4 \Omega/\square$ has a conductivity of 0,38 S/cm. This is better than some films reported in literature, but more than a factor 5 lower than the 2 S/cm reported in literature [14]. Some representative results are reported in the table below.

sample	AV_089	AV_104	AV_106	AV_111
Phase	CAO	CAO	CAO	CAO
$T_{\text{grow}} [^{\circ}\text{C}]$	900	750	750	750
$p\text{O}_2$ [mbar]	0,04	0,004	0,004	0,008
insitu anneal [hrs]	2	3	3	3
Type	-	-	p	p
$R_s [\Omega/\square]$	-	-	$7,43 \cdot 10^4$	$3,54 \cdot 10^5$
σ [S/cm]	-	-	0,38	0,080
T [%]	18	x	-	-
R [%]	3	x	-	-
E_{gap} [eV]	3,2	3,7	-	-

According to XRD-measurements, all thin films in this table consist of CuAlO_2 . The thickness of all samples is estimated to be 354 ± 13 nm, based on XRR-measurements mentioned later. For AV_104 the transmission measurements gave non-physical results due to an improper baseline. A clear slope in the absorptivity to determine the band gap was present.

Hall measurements cannot be performed on these films with the present measurement set-up. The resistance of the films is comparable to the input impedance; therefore the effect can't be measured at low currents. Increasing the currents causes charging of the films, this makes good voltage measurements impossible. A qualitative measurement of the sign of the Seebeck coefficient is a good replacement to determine the type of majority charge carriers.

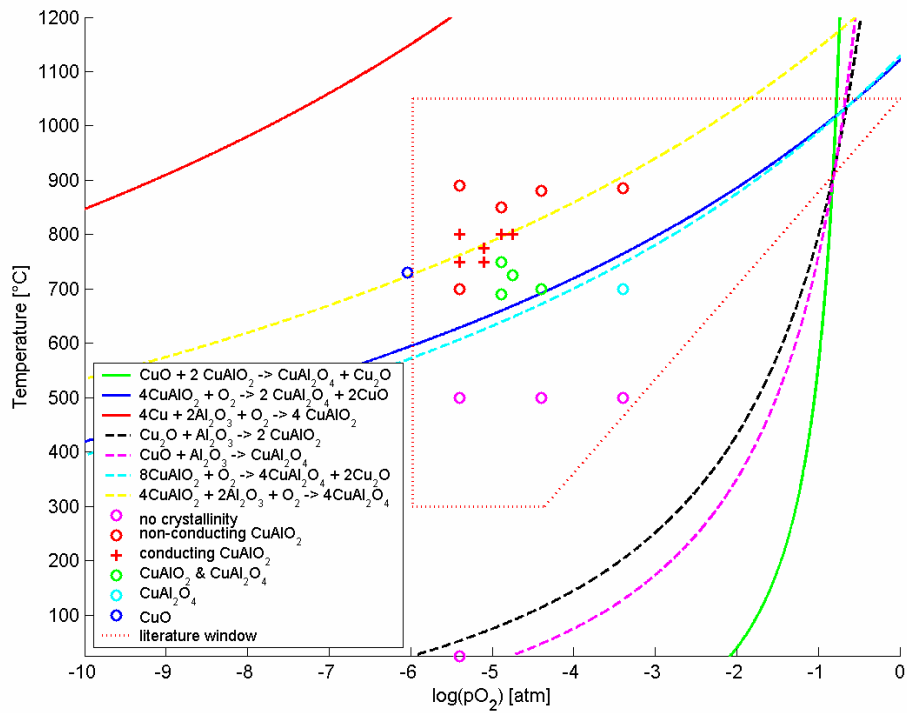


Figure 16: Ellingham diagram of the Cu-Al-O system showing the deposition parameters and phase of deposited thin films.

Transparency measurements are hard to perform, because the substrates had to be glued onto the heater with silver glue. This silver glue can only be removed by polishing the backside of the substrate. However, some silver glue remains on the back of the substrate and some wax is left on the thin film after the polishing process. Therefore there's always some scattering by silver

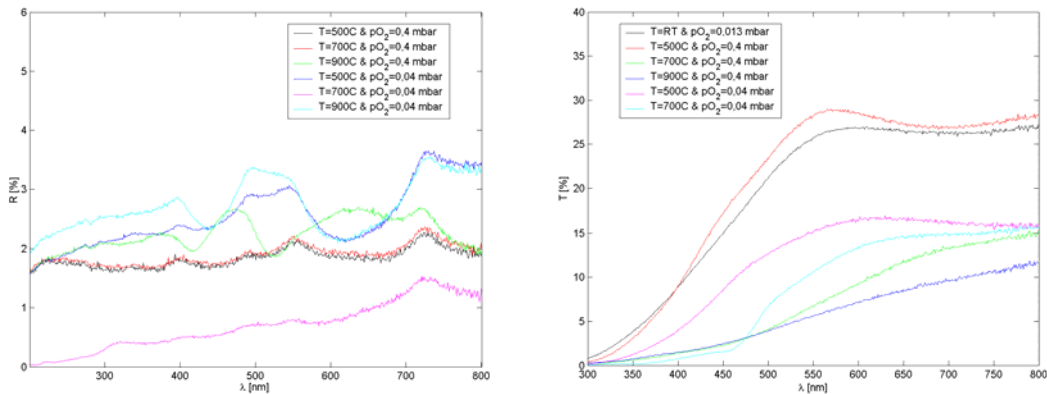


Figure 17: Reflection (left, baseline: bare substrate) and transmission (right, baseline: substrate with silver glue) spectra of in-situ annealed CAO thin films.

particles and wax, causing noise in these measurements. Besides, it's hard to determine a proper baseline to normalize the sample to. Reflection measurements could be performed without polishing. Optical reflectivities of 2 to 6% were measured on unpolished films whereas for polished films this was in the order of 18%. This is probably mainly due to the wax. Also transmission measurements with a substrate with silver glue as a baseline, gave quite good results.

Transmission is low (6 to 24 %) but a clear decrease in transmission for low wavelength is observed. The band gap determined from these measurements differs from 3,3 to 3,9 eV. Which is in good agreement with the band gap of 3,5 eV often found in literature.

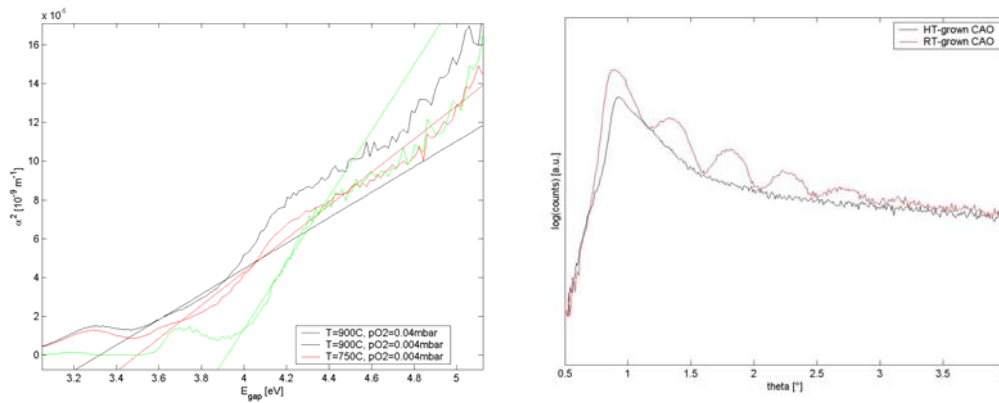


Figure 18: Determination of the optical band gap (left) giving a band gap between 3,2 and 3,9 eV; Thickness determination by XRR (right) showing the X-ray reflection of a crystalline (no fringes) and an amorphous (fringes) CAO film.

The thickness of the thin films could not be determined from the optical measurements. Therefore, X-ray Reflectivity measurements were performed. Because this method only works for rather flat surfaces, measurements were performed on RT-deposited films. Though the thickness measured in this way is that of an amorphous film and not the crystalline CAO, it gives a good indication of the thickness. The thickness of a film grown by ablation with 200 pulses at 10Hz is found to be 98.2 ± 4.4 nm by taking two adjacent maxima or minima. A more distinct result can be obtained by taking a maximum and its second next-neighbour which gives 98.3 ± 2.9 . Based on this data the films deposited during 6 minutes at 20 Hz are estimated to be 354 ± 13 nm.

XRD shows a lot of different phases for different films. Films grown in deposition conditions that are reported in literature ^[30], show the presence of CuAlO_2 and CuAl_2O_4 . This can be explained by the fact that temperature depends on the position where it is measured. In the set-up used in this experiment the heater temperature is measured inside the heater, which can differ from other set-ups. CAO films with a high conductivity show some clear peaks that can only be contributed to CAO. Still there are some films that show the presence of the right CAO phase but show no good characteristics in terms of conduction and transparency (see Figure 16).

For all films the fact that the substrate is one of the possible present phases (Al_2O_3), gives some uncertainty about the film content. Besides all the present phases have XRD-peaks really close to each other making them hard to distinguish.

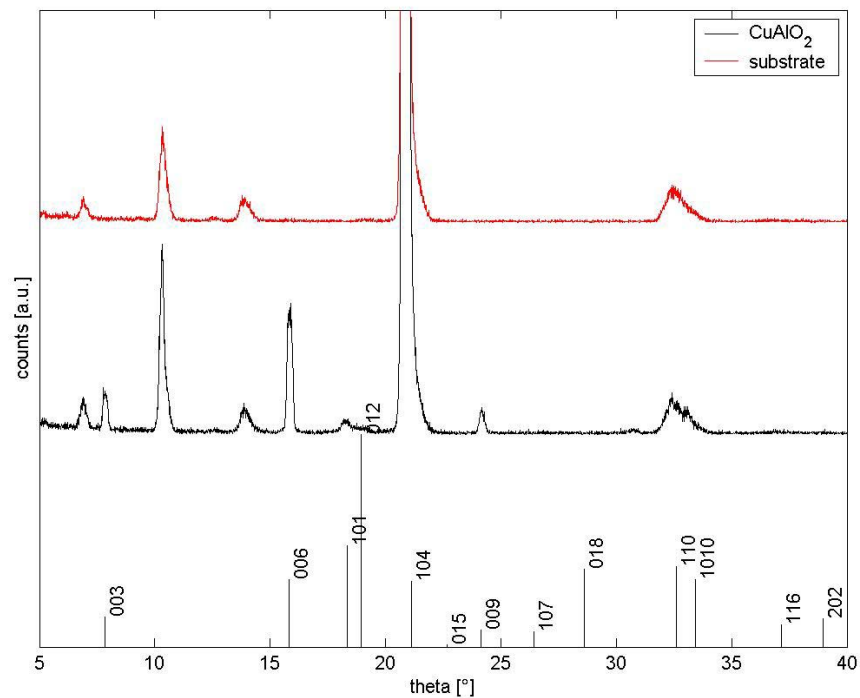


Figure 19: XRD-spectra of sapphire substrate (top), thin CAO film deposited on sapphire (middle) and CAO as reported in literature (bottom).

By relying on the presence of unidirectional peaks like (0 0 3), (0 0 6) and (0 0 9), a reliable particle size analysis of the spectrum is performed. The FWHM-data of the thin film represented in Figure 19 is used to calculate the particle size with the Scherrer-method (formula q). Together with $\lambda = 1.54056\text{\AA}$ and the assumptions that the instrumental broadening is $0,10^\circ$ and the film is strain-free, this leads to:

θ [°]	hkl	counts	θ - [°]	counts	θ + [°]	counts	D [nm]
7.83	(0 0 3)	124	7.72	62	7.98	68	50,1178
15.89	(0 0 6)	372	15.72	191	15.99	179	48,5864
24.19	(0 0 9)	76	24.07	39	24.31	28	62,2056

Thus the peak broadening of the XRD-spectrum indicates a particle size of 54 ± 7 nm. This matches quite well with the crystallites measured with the AFM data. This is shown in Figure 20 and the observed particle size is in the range of 10-100nm.

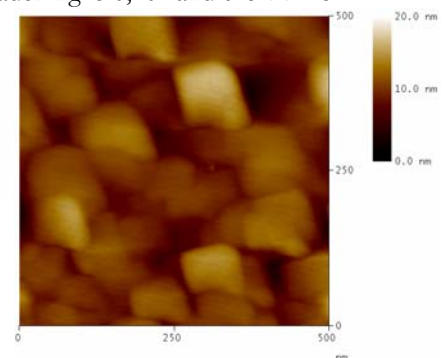


Figure 20: AFM-image of the surface of a CAO thin film showing crystallites.

4.3 Discussion

CAO is a p-type TOS depending strongly on its delafossite crystal structure. In the Cu-Al-O system other crystal phases are formed easily and disturb the conduction. The high kinetic energy of ablated particles does not lead to enhanced crystal formation. Anneals are needed to form crystallites of the delafossite structure. The dependence on temperature and oxygen pressure for films with an in-situ anneal show good correspondence to the Ellingham diagram for bulk.

Different phases, also non-crystalline phases are expected to be present in the thin films. Several films showed only CAO in the XRD-spectrum but had high resistivities. A large amount of grain boundaries or other phases can explain these high resistivities. A large amount of grain boundaries is not very likely as epitaxial growth in the (001)-direction is enhanced by the c-cut sapphire substrates. The observed crystallite size is in the order of 50nm. This is confirmed by the good harmony between peak width analysis of XRD-spectra (54 ± 7 nm) and AFM-analysis (10-100nm). Thus not many grains are present. And although this could not be determined and it is not expected for the high growth temperatures, the presence of amorphous phases could be a reason for the low conductivity.

Further improvement of the growth parameters is expected because the conductivity is a factor 5 lower than the best films reported in literature ^[14]. For the Hall measurement set-up, the resistivity is higher than the input impedance of the measurement system. This problem can be solved because the resistance of these films is in the order of $M\Omega$.

It can be expected that the measured transparencies are lower than the actual values. This is due to the silver glue. And based on the measured band gap of 3,2-3,9 eV, higher transmissions can be expected. This observed band gap is in good agreement with literature.

A reliable thickness is obtained from XRR-measurements. A small difference will exist between the amorphous and the crystalline film. But the difference is expected to be small, because the deposition rate is not temperature dependent.

5 ZincRhodiumOxide (ZRO)

ZRO is a recently (2001) discovered p-type amorphous TOS [21]. The only publications on ZRO thin films are by the group of H. Hosono [21]-[23] whose best results are thin films with a band gap of 2,1 eV and an associated indirect band gap of 1,1 eV (see Appendix 8.1) and a conductivity of $1,9 \text{ S cm}^{-1}$ [22],[23]. This group performs thin film depositions by sputtering, whereas the films in this research are deposited by PLD. First the characterization of the target is described here, followed by the result of the first depositions with PLD.

5.1 Preparation

ZRO is deposited at RT and at 700°C to grow crystalline films. Quartz substrates are used because quartz can handle temperatures up to 700°C . Before use, the $5 \times 5 \text{ mm}$ quartz substrates were ultrasonically cleaned in acetone and rinsed with ethanol.

5.1.1 Target

The target (prepared according to the procedure described in section 2.1.3) was analysed with the X-ray diffractometer. The powder diffractogram of the target shows very good correspondence to that found in literature (Figure 21), indicating a good stoichiometry.

5.1.2 Pulsed Laser Deposition

Thin films of ZRO are produced by PLD with the settings mentioned in the table on the next page. First the right energy density for homogeneous ablation was determined. As shown in Figure 22 no pillars are formed for an energy density of 4 J/cm^2 and the ablation seems homogeneous.

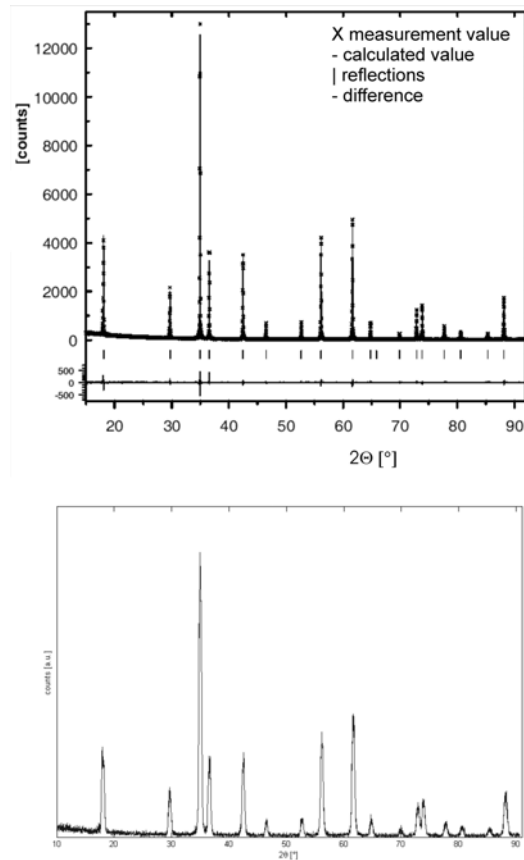


Figure 21: Powder diffractogram of ZnRh_2O_4 from reference [25] (top) and as measured from the prepared target (bottom).

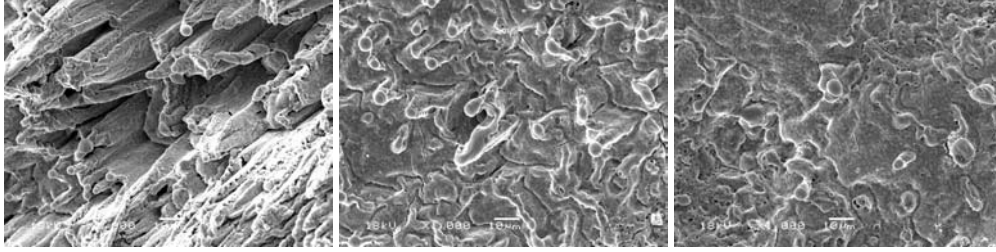


Figure 22: SEM-images of ablated surfaces of a ZRO-target. The energy density on the target varies from 2 J/cm^2 on the left via 3 J/cm^2 in the middle to 4 J/cm^2 on the right.

Experimental details: first PLD-settings

spot size	$2,1 \text{ mm}^2$
energy density	4 J/cm^2
temperature	RT and 700°C
background pressure	$4 \cdot 10^{-6} - 1 \cdot 10^{-5} \text{ mbar}$
process pressure and gas	$0,003\text{-}0,100 \text{ mbar O}_2$, some mixed with Ar
substrate	quartz
targets	ZRO

The oxygen pressure for the first experiments is relatively low. It is based on the oxygen pressure used by Narushima [23]. Because no oxygen vacancies should be present, depositions at higher oxygen pressures could show better electrical and optical properties. No experiments at high(er) oxygen pressures are performed yet.

5.2 Results

Only a few depositions and measurements on the obtained samples have been performed. Depositions at 700°C on c-cut sapphire show crystalline film growth (Figure 23). Whereas no or hardly any crystallinity seems to be present in films deposited at 700°C and RT on quartz. But the surface of RT-grown thin films shows a certain structure. AFM-measurements on these samples show particles of approximately 300 nm (Figure 24).

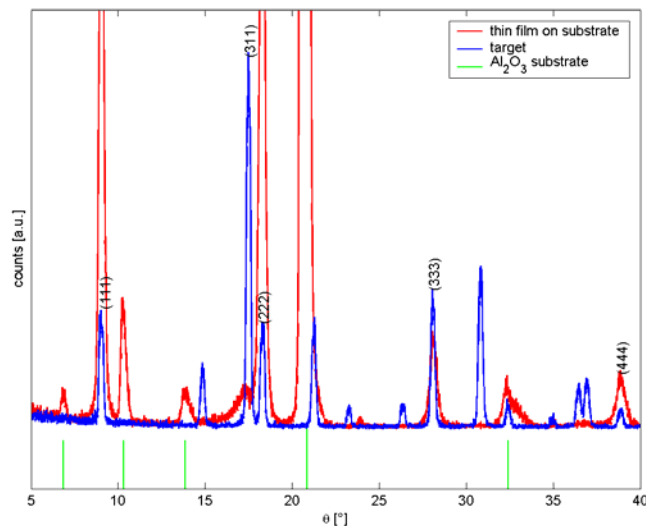


Figure 23: XRD-spectra of ZRO target (blue), thin film on a Al_2O_3 substrate (red) and the Al_2O_3 substrate (green).

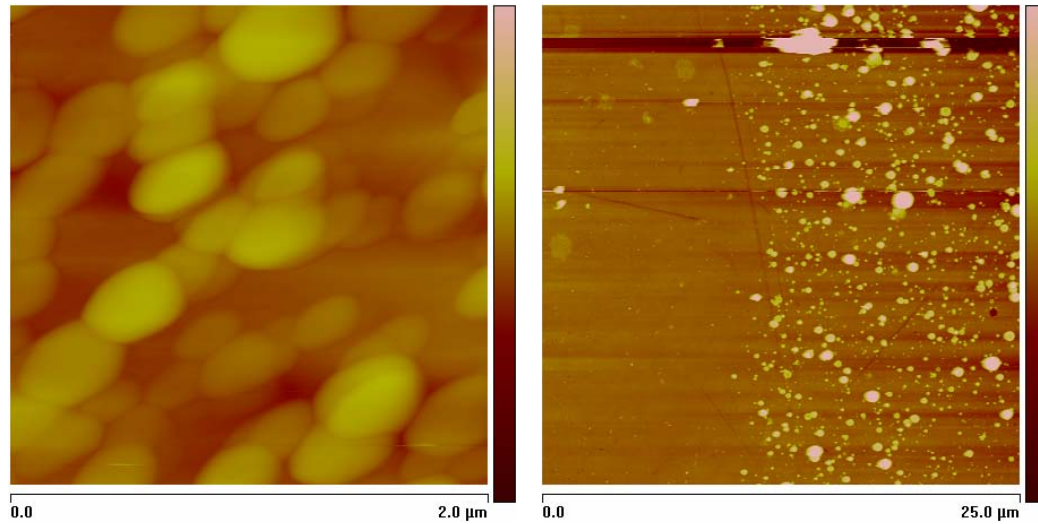


Figure 24: AFM height images of RT-deposited ZRO showing particles (full z-scale 300nm, left) and a step edge (full z-scale 150nm, right).

On only a few ZRO samples resistivity measurements have been performed. The lowest sheet resistance of 1,1 k Ω was measured on a film deposited at 700°C and 0,100 mbar pO₂ on c-cut sapphire. For films grown in the same circumstances on quartz, the sheet resistance approximately doubled to 2,5 k Ω . For films grown on quartz at RT, the resistance was approximately a factor 15 higher than those grown at 700°C. Seebeck measurements on films grown at 700°C show p-type conductivity.

Figure 24 (right) shows that the film thickness can't be determined with an AFM. Since particles have formed along the step-edge in the PLD-process. The optical transmission spectrum of ZRO (Figure 25 (left)) shows no clear fringes, thus no thickness information is available. For comparison, the transmission spectrum of ZRO in Figure 25 is shown together those of ITO and CAO. Transmission spectra of ZRO thin films show an optical transmission ranging from 50 to 59% and reflection of approximately 6%.

The band gap determined from the reflection and transmission spectrum is shown in the right image of Figure 25 and results in a band gap of 2.1 eV. But it could also be lower, down to 1,8 eV. The indirect band gap reported in literature [22] has not been determined.

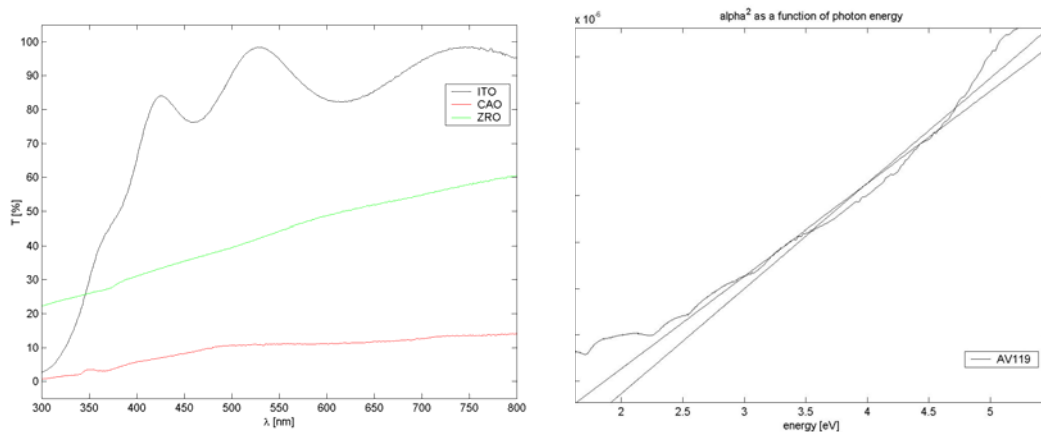


Figure 25: Transmission spectra of ITO, CAO and ZRO (left); band gap determination of ZRO.

5.3 Discussion

The dependence of the electrical and optical properties of ZRO on its crystal structure seems to be not very strong. From a polycrystalline to a nanocrystalline phase the resistivity approximately doubles. The change from nanocrystalline growth at 700°C to nanocrystalline growth at RT is a factor 15. This last difference is rather large and indicates a large difference between different nanocrystalline states.

As AFM images of RT-deposited film show particles, some structure could be present. The particles indicate either ablation of entire particles or particle formation in the plasma phase or on the substrate. Ablation of entire particles is not expected, as the ablation is homogeneous (Figure 22). Thus particles could be formed in the plasma or on the substrate.

It is interesting to determine the dependency of the amorphous p-type TOS ZRO on the presence of oxygen vacancies. The n-type amorphous TOS ITO shows strong dependency on the presence of oxygen vacancies, this is not determined yet for ZRO.

6 Conclusions

In this chapter, first the specific conclusions on the successively investigated materials will be given. This is followed by some general conclusions and recommendations on PLD-growth and characterization of TOSs.

The crystal structure is not necessary for the electrical conduction in ITO. Also for transparency the structure is not needed, but it has some influence on the optical properties.

Besides growth temperature, the oxygen pressure is an important parameter in the determination of the thin film properties. The oxygen pressure in the deposition process is related to the oxygen vacancies in the thin film. Increasing the oxygen pressure decreases the oxygen vacancies and vice versa. As this oxygen pressure strongly influences the electrical and optical properties of ITO, oxygen vacancies play an important role in the conduction.

Also the dopant (Sn at In-sites) can be an important parameter for the electrical properties. For polycrystalline films doping increases the charge carrier density. The properties of amorphous (Sn:)In₂O₃ are not improved by doping.

CAO shows a strong dependency on its crystal structure for TOS-properties. Besides, the Cu-Al-O system shows a lot of possible crystal phases of which only CuAlO₂ in the delafossite structure has the desired properties. Therefore the set of conditions to grow this phase is very narrow and low temperature deposition is impossible.

CAO is a p-type TOS with a band gap between 3,3 and 3,9 eV. The thin films made by PLD show a conductivity of 0,38 S/cm. This means clearly lower charge carrier density and mobility than most n-type TOSs. It is thought that besides fundamental differences, this is caused by present amorphous phases that disturb the crystalline structure. Also grain boundaries could play a role. Both explanations support the idea that CAO is a polaron conductor.

So CAO is a p-type TOS, but the 2D-structure of the copper planes is not very useful because it is very rapidly disturbed in non-ideal growth. Methods to decrease the growth temperature, like mixing gasses, were unsuccessful. A substrate with a very good lattice match was used, facilitating epitaxial growth. Adding a dopant like Mg or Be as sometimes proposed in literature [19], probably complicates the phase diagram even more. It is not expected that this enhances the properties of CAO.

P-type TOS properties of ZRO are not merely determined by its crystal phase. Also amorphous ZRO shows semiconductivity and transparency. The difference in conductivity from a crystalline to an amorphous phase is only a factor 2. From first depositions of ZRO the band gap seems to be approximately 2 eV and the sheet resistance is in the kΩ-range.

PLD-grown amorphous ZRO shows no crystallinity but a certain structure is observed: its surface consists of particles of approximately 300nm in size. The formation and role of these particles is unclear.

Some experiments to form a p/n-junction with ITO on CAO have been performed. But these were unsuccessful up till now: resistor-behaviour was observed. A good match of the properties of the p- and n-material seems to be inevitable. With a good knowledge of ITO and ZRO, further research on this can lead to an amorphous transparent p/n-junction. Therefore further research on ZRO is proposed.

For the characterization of these films, Hall measurements of highly resistive films are needed. In the current set-up this is difficult: either charging occurs or the Hall effect is too small to measure. A measurement set-up with higher input impedance can solve this problem. This can also improve the van der Pauw set-up. The Seebeck set-up used now is quite simple and a well-controlled temperature gradient can improve the understanding of the observed effects.

7 Literature list

- [1] J. Als-Nielsen (1987). In W. Schommers and P. von Blanckenhagen. *Structure and Dynamics of Surfaces II*. Berlin: Springer-Verlag. pp. 181.
- [2] N.W. Ashcroft and N.D. Mermin (1976). *Solid State Physics*. London: Thomson Learning, Inc.
- [3] K.S. Birdi (2003). *Scanning probe microscopes: applications in science and technology*. Boca Raton: CRC Press.
- [4] A. Buljan, P. Alemany and E. Ruiz (1999). *Electronic structure and bonding in CuMO_2 ($M=\text{Al, Ga, Y}$) delafossite type oxides: an ab initio study*. J. Phys. Chem. B 103, pp. 8060-8066.
- [5] H.B. Callen (1985). *Thermodynamics and an introduction to thermostatistics*. New York: John Wiley & Sons, Inc.
- [6] D.P. Cann and B. Gall (2004). *Electrical properties of n- and p-doped CuGaO_2 with the delafossite structure*. <http://mse.iastate.edu/electroceramics/downloads/Nashville3.pdf> .
- [7] D.B. Chrisey and G.K. Hubler (1994). *Pulsed laser deposition of thin films*. New York: John Wiley & Sons, Inc.
- [8] J.M. Dekkers. Article to be published.
- [9] A.M.M. Gadalla and J. White(1964). *Equilibrium relationships in the system $\text{CuO-Cu}_2\text{O-Al}_2\text{O}_3$* . Transactions of the British Ceramic Society 63(1), pp 39-62.
- [10] L. Gmelin (1924). *Gmelin Handbuch der Anorganischen Chemie*. Cu 60 Tl. B Lfg 3. Berlin: Springer. pp 1169-1172
- [11] G. Gonzalez (2003). *Defect structure studies on indium tin oxide using x-ray and neutron diffraction techniques*. <http://www.matsci.northwestern.edu/faculty/links/tom/gabyresearch.htm> .
- [12] I. Hamberg and C.G. Granqvist (1986). *Evaporated Sn-doped In_2O_3 films: Basic optical properties and applications to energy-efficient windows*. J. Appl. Phys. 60(11), pp R123-R159.
- [13] A.R. Hind and L. Chomette (2003). *The determination of thin film thickness using reflectance spectroscopy*. <http://www.varianinc.com/image/vimage/docs/products/spectr/uv/atworks/uv90.pdf>
- [14] B.J. Ingram et al. (2001). *Electronic structure and small polaron hole transport of copper aluminate*. Physical Review B, Vol. 64, 155114.
- [15] K.T. Jacob and C.B. Alcock (1975). *Thermodynamics of CuAlO_2 and CuAl_2O_4 and phase equilibria in the system $\text{Cu}_2\text{O-CuO-Al}_2\text{O}_3$* . Journal of The American Ceramic Society Vol. 58 No. 5-6, pp 192-195.
- [16] M. Kanzari and B. Rezig (2000). *Effect of deposition temperature on the optical and structural properties of as-deposited CuInS_2 films*. Semiconductor Science Technology 15, pp. 335-340.
- [17] H. Kawazoe et al. (1997). *P-type electrical conduction in transparent thin films of CuAlO_2* . Nature 389, pp 939-942.

- [18] H.P. Klug and L.E. Alexander (1954). *X-ray diffraction procedures*. New York: John Wiley & Sons, Inc.
- [19] T. Koyanagi et al. (2003). *Materials design of p-type transparent conducting oxides of delafossite CuAlO_2 by super-cell FLAPW method*. Journal of Phys. and Chem. of Solids 64, pp. 1443-1446.
- [20] Materials Research Society (2000). *MRS Bulletin Volume 25, No. 8*.
- [21] H. Mizoguchi et al. (2001). *ZnRh_2O_4 : A p-type semiconducting oxide with a valence band composed of a low spin state of Rh^{3+} in a $4d^6$ configuration*. Appl. Phys. Lett. 80(7), pp. 1207-1209.
- [22] S. Narushima et al. (2003). *A p-type amorphous oxide semiconductor and room temperature fabrication of amorphous oxide p-n heterojunction diodes*. Advanced Materials 15 No. 17, pp 1409-1413.
- [23] S. Narushima et al. (2003). *X-ray amorphous p-type conductive oxide; ZnRh_2O_4* . Mat. Res. Soc. Symp. Proc. Vol. 747, V2.2.1-6.
- [24] NIST (2002). *Hall effect measurements*. <http://www.eeel.nist.gov/812/effe.htm> .
- [25] C. Renkenberger (2004). *Neue oxidische Rhodiumverbindungen: Syntheseveruche und strukturelle Untersuchungen*. Heidelberg: Doctoral dissertation Ruprecht-Karls University.
- [26] D.B. Rogers et al. (1971). *Chemistry of noble metal oxides. III. Electrical transport properties and crystal chemistry of ABO_2 compounds with the delafossite structure*. Inorganic Chemistry 10(4), pp. 723-727.
- [27] I.S. Shaplygin and V.B. Lazarev (1980). *Preparation, properties and infrared spectra of the spinels MRh_2O_4 (represents a group II element)*. Russ. J. of Inorg. Chem. 25(4), pp. 906-909.
- [28] R.E. Stauber et al. (1999). *Thin film growth of transparent p-type CuAlO_2* . Electrochemical and Solid-State Letters 2 (12), pp 654-656.
- [29] N. Tsuboi et al. (2003). *Delafossite CuAlO_2 films prepared by reactive sputtering using Cu and Al targets*. Journal of Physics and Chemistry of Solids 64, pp 1671-1674. <artikel met variatie in Cu en Al>.
- [30] H. Yanagi et al. (2000). *Electronic structure and optoelectronic properties of transparent p-type conducting CuAlO_2* . Journal of Applied Physics 88 (7), pp 4159-4163.
- [31] M. Yoshimoto et al. (1995). *Atomic-scale formation of ultrasmooth surfaces on sapphire substrates for high-quality thin-film fabrication*. Appl. Phys. Lett. 67 (18), pp 2615-2617.

8 Appendix

8.1 Optical band gap determination

Starting from the basic formula that the sum of the absorption, reflection and transmission is 1, and with the definition of the absorption coefficient, one can write:

$$A + R + T = 1$$

$$A = 1 - R - T$$

$$R + T = e^{-\alpha d}$$

where d is the thickness of the film. The error in this formula can be considerable, because it doesn't take reflections under the surface of the film into account.

Therefore, we will use the approximation formula

$$T \approx (1 - R)^2 e^{-\alpha d} \Leftrightarrow \alpha = \frac{1}{d} \ln \left(\frac{(1 - R)^2}{T} \right)$$

And because the absorption coefficient α is related to the optical bandgap E_g by the equation

$$\alpha(h\nu) \propto \frac{(h \cdot \nu - E_g)^n}{h \cdot \nu}$$

$$\alpha(h\nu) \cdot h \cdot \nu \propto (h\nu - E_g)^n$$

$$(\alpha(h\nu) \cdot h \cdot \nu)^{1/n} \propto h\nu - E_g$$

with α the absorption coefficient, h Planck's constant and n equal to 1/2 for a direct gap, 2 for an indirect gap and 3/2 for a forbidden direct transition. Since this can be written in the form $y=x-a$ and we want to determine a, the y-axis intercept has to be determined. Since the equation above is not valid over the entire energy range, the incline of the tangent is determined for a specific region and its intercept with the y-axis is determined.

Because it is known that most TOSs are direct gap semiconductors, the band gap to be determined is

$$\alpha h\nu = A(h\nu - E_g)^{1/2}$$

$$\left(\frac{\alpha h\nu}{A} \right)^2 = h\nu - E_g$$

So α^2 is plotted as a function of the energy $h\nu$, which should give, at least in the energy region for which the material is a direct gap semiconductor, a linear relation. And finally the optical band gap is thus obtained by fitting a straight line to the plot and determining its energy-axis intersection ($\alpha^2=0$, so this gives the band gap energy E_g).

Also the indirect gap and forbidden direct transition can be determined by plotting $\alpha^{1/2}$ respectively $\alpha^{2/3}$ as a function of energy [16].

8.2 Crystal structures

Listed are the most elemental data of the encountered crystal structures.

material	structure	Group	a [Å]	b [Å]	c [Å]	remarks
In ₂ O ₃	Ia3	cubic	10,105			
SnO ₂	P4 ₂ /mnm	tetragonal	4,7382		3,1871	
Al ₂ O ₃	R-3c	hexagonal	4.763		13.003	
CuAlO ₂	R-3m	hexagonal	2.8604		16.953	
CuO	C2/c	monoclinic	4.6837	3.4226	5.1288	$\beta = 99.29^\circ$
Cu ₂ O	Pn3m	cubic	4.2685			
CuAl ₂ O ₄	Fd3m	cubic	8.078			
Cu ₂ Al ₄ O ₇ *	F-43m	cubic	8.09			
ZnO	P6 ₃ mc	hexagonal	3,250		5,207	
Rh ₂ O ₃	R-3	hexagonal	5,208		14,155	
ZnRh ₂ O ₄	Fd3m	cubic	8,5085			few publications

*in old literature Cu₂Al₄O₇ is found, in newer literature this phase is not mentioned, but tetragonal CuAl₅O₈ is mentioned.